Analysis of a No-Insulation HTS Pancake Coil Including Multiple Resistive Joints

A. Musso, J. Bang, U. Bong, M. Breschi, C. Im, G. Kim, J. Kim, J. Park, and S. Hahn

***Abstract*—One of the technical issues in the application of High Temperature Superconducting (HTS) tapes to magnet technology is the need to wind long tape sections with uniform electric properties along the length. It has been reported that a No-Insulation (NI) coil can properly work even in the presence of defective super-conductive regions, with a minimal drop of performance as com-pared to its "defect-free" counterpart. This could open up the possibility of manufacturing coils by jointing together several tape segments of limited length, lowering the conductor cost. In this work, a single pancake NI HTS coil is wound using several tape segments cut from the same lot, jointed together. The electrical resistance of each joint is set independently, realizing either high or low resistance joints. Thus, the coil is designed to include multiple defective sections at specific locations. The coil is refrigerated by conduction-cooling, and tested at different temperatures and charging rates. The coil instrumentation allows measuring the voltage over the whole winding, as well as the magnetic field in the central bore. The measurements are used to study the defect-irrelevant behavior of the coil. A simple equivalent lumped parameter circuit is applied to derive the coil effective parameters and analyze its electromagnetic behaviour.**

***Index Terms*—Equivalent circuits, High Temperature Superconductors, No-insulation coils, Superconducting coils.**

I. Introduction

In THE recent years, the No-Insulation (NI) winding technique is emerging as a valid alternative to conventional High Temperature Superconductor (HTS) insulated coils [1]–[3]. The absence of electrical insulation between turns allows the operating current to flow radially, thus avoiding damaged areas [1]–[3]. In the literature, it has been demonstrated how NI windings can work properly even in the presence of defects along the conductor length [1]–[3]. An effective current and temperature redistribution in the winding improves the NI coil thermal stability, compared to its insulated counterpart [1]–[3].

On the other hand, in insulated coils, no alternative path is possible for the current apart from the longitudinal one. Their performance is strongly affected by the presence of local defects, and their operating limits are set by the conductor sections exhibiting the lowest performance. Thus, the tape should have uniform electric properties along its length, and be purchased in long and more expensive lengths to reduce the number of resistive joints inside the winding.

This work aims to analyze the operation of a single-pancake NI HTS coil realized with multiple joints of different extension, intentionally inserted between different tape lengths before the winding phase. Accidentally, one of the joints inserted in the coil was damaged during the tests. Should such a damaged section be introduced in an insulated coil, it would require to substitute a section or the entire winding. Charge-discharge cycles are performed at different ramp rates, up to 5 A/s, as well as fast discharge tests. Compared to the results reported in [13], where the same coil was operated in a liquid nitrogen bath, in this work the tests are carried out with conduction cooling, at temperatures between 4.7 K and 80 K. The coil electromagnetic behavior is assessed by measuring the magnetic field produced in its bore and the voltage signal acquired at the coil ends. The measurements are also used to retrieve, by means of a simplified lumped parameter circuit, some useful effective parameters, such as the longitudinal and radial resistances, from which the fraction of operating current flowing radially throughout the winding is estimated.

TABLE I
Tape and Winding Parameters

Tape width ; thickness [mm]	4.1 ; 0.145
Tape I_c ; n-value (at 77 K and s.f.)	255.4 A ; 46
Coil i.d. ; o.d. [mm]	40.1 ; 53.4
Number of turns	46
Total conductor length [m]	6.71
Length of 1st; 2nd; 3rd joint [cm]	4.0 ; 6.0 ; 8.0
Location of 1st; 2nd; 3rd joint (along the conductor) [m]	1.97 ; 3.36 ; 5.74
Location of 1st; 2nd; 3rd joint (inside the coil) [turn]	15th ; 24th ; 39th
Resistance of 1st; 2nd; 3rd joint before winding [μΩ·cm]	7.0 ; 9.0 ; 7.3
Resistance of 1st; 2nd; 3rd joint after disassembly [μΩ·cm]	8.1 ; 16.5 ; 1258.8

II. Experimental Setup

The *SuNAM SCN04150* tape is selected for this work; its geometric and electrical properties are reported in Table I [27]. From the data provided by the manufacturer, the critical current variations along the total conductor length utilized in this work are limited below 1.5%. For the purpose of this analysis, it is relevant to start from a tape characterized by highly uniform properties, so that the only defects within the coil are those intentionally inserted through the joints. First, the tape length is cut into four segments of 200, 138, 240 and 141 cm, used in

Manuscript received 29 November 2021; revised 11 March 2022; accepted 29 April 2022. Date of publication 5 May 2022; date of current version 19 May 2022. This work was supported by the Korea Medical Device Development Fund grant funded by the Korean government under Projects 1711138068, KMDF_PR_20200901_0063. *(Corresponding author: Andrea Musso.)*

A. Musso and M. Breschi are with the Department of Electrical, Electronic, and Information Engineering, University of Bologna, 40136 Bologna, Italy (e-mail: andrea.musso3@unibo.it).

J. Bang, U. Bong, C. Im, G. Kim, J. Kim, J. Park, and S. Hahn are with the Department of Electrical and Computer Engineering, Seoul National University, Seoul 08826, Republic of Korea.

Color versions of one or more figures in this article are available at https://doi.org/10.1109/TASC.2022.3172927.

Digital Object Identifier 10.1109/TASC.2022.3172927

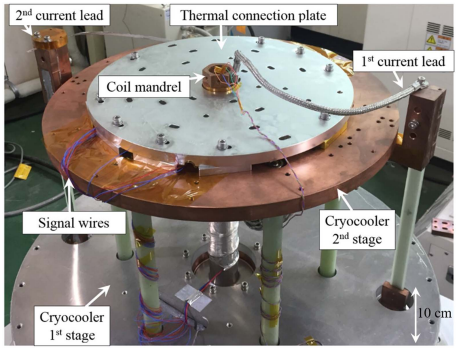

Fig. 1. Experimental setup for the coil connection to the cryogenic system, showing current leads and wires for the signal acquisition.

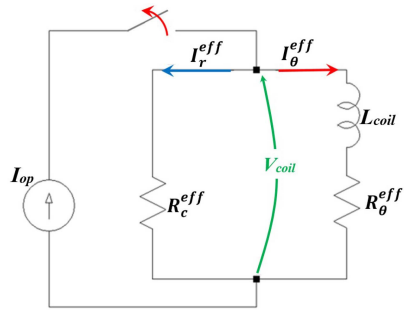

Fig. 2. Equivalent lumped parameter circuit for a NI pancake-wound coil.

this order to wind the turns from the inner to the outer radius of the pancake. These lengths include the overlapping tape portions between adjacent segments, necessary to realize the joints. They are set so that the resulting joint locations after the winding phase are sufficiently spaced in terms of both radial and azimuthal distance inside the coil, as shown in Table I.

The segments are jointed together by applying a lap joint procedure [28]. In order to obtain a different resistance at each joint, the length of the overlapping portion is varied, as reported in Table I. The joints are numbered from 1 to 3, going from the innermost to the outermost one in the winding. Then, the joint resistances are measured in liquid nitrogen bath. Their values, multiplied by the corresponding joint lengths, are also reported in Table I. The measurements were performed both before the winding of the pancake and after the coil disassembly, at the end of the test campaign. Before the winding phase, the resistance values are rather similar for the 3 joints. After the coil disassembly, they increase by factors 1.17, 1.83, and 173 compared to the previous measurements, for the 1st, 2nd and 3rd joint respectively. In particular, the 3rd joint might have been damaged at an intermediate stage (winding or unwinding phases, for example), since its resistance reaches 157.4 $\mu\Omega$, a value much greater than that of the other joints. Since it was not possible to detect the joint resistances during the coil tests, the values measured after the coil disassembly are assumed as valid for the whole testing phase.

Subsequently, the tape is wound in a single-pancake configuration and connected to the power supply. One current lead is screwed to the mandrel itself, made of highly conductive copper. The innermost turn of the coil is soldered to the mandrel outer surface, ensuring a regular current flow. The coil is instrumented with a pair of voltage taps soldered at the coil ends (excluding the tape segments connected to the terminations). A Hall sensor, is placed at the central axis of the coil bore, to monitor the axial magnetic field of the coil during the tests. The active surface of the sensor is placed 7 mm higher than the center line of the winding. Then, the signal wires are connected to a *NI SCXI-1125* acquisition card [30].

Finally, the coil mandrel is fixed to the 2nd stage of a GM cryocooler, as shown in Fig. 1. To ensure a better thermal contact, a circular metal plate is pressed above the coil and thermally connected to the cryocooler 2nd stage. The coil temperature, measured by a thermocouple during tests, is varied by activating a heater attached to the 2nd stage. The NI coil is first charged at different ramp rates, up to an operating current (I_{op}) of 70 A. The current is kept at its peak ($I_{op}^{\max}$) for several seconds, to reach the steady-state conditions. Then, the coil is discharged with the same rate used for the charging or discharged rapidly, depending on the test. The experiments are repeated varying $I_{op}^{\max}$ and at temperatures between 4.7 K and 80 K.

III. Equivalent Circuit

In the literature, different approaches are proposed to investigate the behavior of NI coils, mainly based on equivalent distributed [12]–[14], [31]–[33] or lumped [34]–[39] parameter circuit models. In this work, the NI pancake-wound coil is characterized using the simple equivalent lumped parameter circuit shown in Fig. 2. In this circuit, I_{op} is the total coil transport current, I_θ^{eff} is the current flowing longitudinally through the winding and the resistance R_θ^{eff}, which accounts for both the superconductor resistance and the resistance of the defective areas. I_r^{eff} represents the current flowing radially through the turn-to-turn resistance of the coil R_c^{eff}. In the circuit, I_{op} is the sum of I_θ^{eff} and I_r^{eff}. V_{coil} corresponds to the total coil voltage measured at its terminals. An opening switch is also inserted in the circuit to study fast discharge tests.

The parameters of this model should be regarded as *effective* values, since they describe the macroscopic coil behavior other than local conditions within the winding. The scope of this analysis is to compare the coil effective parameters at the different test temperatures. For the sake of comparison, the parameter values are computed at a fixed time instant t_r, when I_{op} equals $I_{op}^{\max}$ and the steady-state conditions are reached.

Thus, the contribution of the coil inductance (L_{coil}) to $V_{\text{coil}}(t_r)$, measured at time t_r, can be neglected. It results that $V_{\text{coil}}(t_r) = R_\theta^{eff} \cdot I_\theta^{eff} = R_c^{eff}(t_r) \cdot I_r^{eff}(t_r)$. This allows to compute analytically the model parameters as shown in (1). It is worth noting how L_{coil} is still required to solve (1). In fact, it enters in the definition of the coil characteristic time (τ), as $\tau = L_{\text{coil}}/(R_c^{eff} + R_\theta^{eff})$. This equation is needed to solve the equivalent circuit. While τ is experimentally determined from the rapid discharge tests, L_{coil} is computed analytically. The winding is approximated as a single conductor with rectangular cross-section, included between the inner and the outer radius of the winding. The value obtained for L_{coil} is 150.6 μH.

$$\begin{cases} I_r^{eff}(t_r) = \dfrac{I_{op}(t_r) - \sqrt{I_{op}(t_r)2 - \frac{4\,\tau\,V_{\text{coil}}(t_r)\,I_{op}(t_r)}{L_{\text{coil}}}}}{2} \\ I_\theta^{eff}(t_r) = I_{op}(t_r) - I_r^{eff}(t_r) \\ R_c^{eff}(t_r) = V_{\text{coil}}(t_r) \,/\, I_r^{eff}(t_r) \\ R_\theta^{eff}(t_r) = V_{\text{coil}}(t_r) \,/\, I_\theta^{eff}(t_r) \end{cases} \tag{1}$$

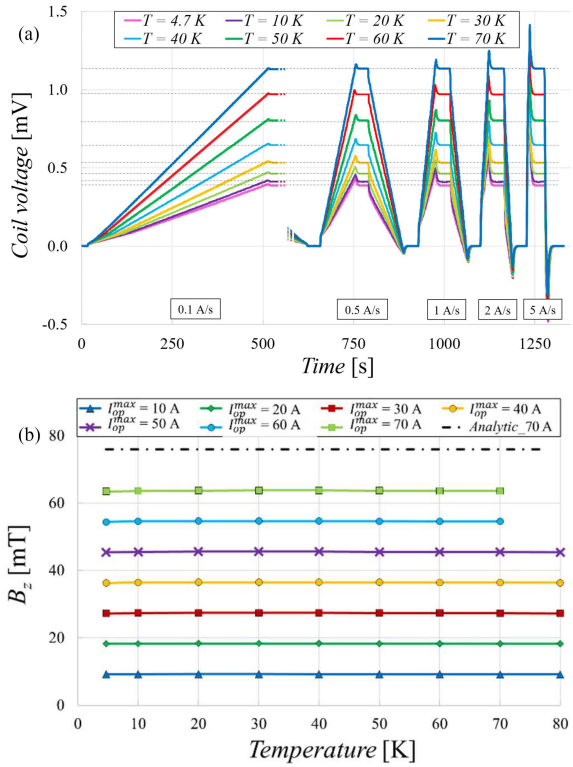

Fig. 3. (a) Voltage profile measured during charging-discharging tests at different ramp-rates and temperatures. (b) Maximum magnetic field measured during tests at different $I_{op}^{\max}$ values and temperatures.

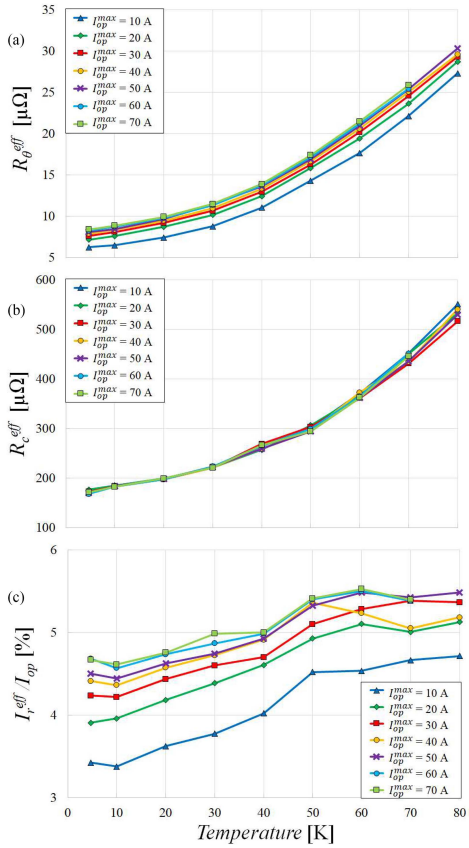

Fig. 4. (a) R_θ^{eff}, (b) R_c^{eff} and (c) I_θ^{eff}/I_{op} parameters computed at $t = t_r$ for different $I_{op}^{\max}$ values and temperatures.

IV. Results and Discussion

A. Experimental Measurement From Charging Tests

It is known that NI coils usually require a slow charging procedure [40]–[47], due to the radial currents which can flow even at low operating currents, thus affecting the coil operation (*e.g.*, producing a relevant heat dissipation). To estimate how fast the defective NI coil can be safely charged, consecutive charge-discharge tests are performed, increasing the ramp-rate (0.1 A/s, 0.5 A/s, 1 A/s, 2 A/s and 5 A/s) up to the same peak current (70 A). The test is repeated at different temperatures. Fig. 3(a) presents the voltage profiles acquired during the experiments. To improve readability, the discharges at 0.1 A/s are not displayed. It is worth noting that the amplitude of the voltage obtained at steady state during the flat top of the current cycle ($I_{op} = I_{op}^{\max}$) remains the same for every ramp-rate (horizontal dashed-lines show these values at each temperature). Inductive transients are visible at the beginning and at the end of the charge and discharge phases. Although the amplitude of the inductive peaks increases with increasing the ramp-rate, the coil works properly and it can be charged and discharged safely up to 5 A/s.

Fig. 3(b) shows the trend of the maximum magnetic field measured during tests carried out up to the same $I_{op}^{\max}$, varying the operating temperature. The magnetic field appears constant with temperature (variations are below 0.8%) and proportional to the current supplied, a sign that the coil is performing well, despite the presence of defects. This is a relevant result, assuming valid the presence of the damaged section (3rd joint) within the coil, the coil can still be operated at various conditions of ramp rate, temperature and peak transport current. In an insulated coil, the presence of such a damaged joint would require replacing this section or the entire winding.

The magnetic field generated by a defect-free coil having the same geometrical properties of the test coil, computed analytically as in [48], at $I_{op}^{\max}$= 70 A and at the Hall sensor location, is displayed in Fig. 3(b) as a black dashed line. The analytical calculation considers the current density as uniformly distributed over the cross-section of the winding. The measured magnetic field at $I_{op}^{\max}$= 70 A is 16.5% lower than the one computed for its defect-free counterpart, indicating that the presence of defective joints affects the total magnetic field produced. However, it should be noted that even a small misalignment in positioning the Hall sensor active surface at the central axis of the coil, may have led to an underestimation of the measured field.

B. Temperature Dependence of the Coil Parameters

In order to solve (1), the time constant τ is determined from the fitting of the voltage measured during the current dump. It results that τ decreases linearly with increasing the temperature, from 832 ms at 4.7 K, to 259 ms at 80 K.

Fig. 4(a) shows the parameter R_θ^{eff} computed at steady state conditions, for the tests performed up to a given $I_{op}^{\max}$ and varying the temperature. R_θ^{eff} increases non-linearly with temperature. Moreover, R_θ^{eff} does not correspond to the sum of the resistances measured for the 3 joints (as it would be in an insulated coil), although the order of magnitude is respected. This result could be explained by a combination of two different phenomena: specific tape sections might be approaching

their critical current and the joint resistances also increase with temperature.

Fig. 4(b) presents the parameter R_c^{eff} computed at $t = t_r$, for the same cases shown in Fig. 4(a). Its values increase non-linearly with temperature; the dependence resembles that of the copper resistivity vs temperature curve [49]. It should be recalled that, in the proximity of the joints, the current I_r^{eff} flows radially through the copper layers of the tape and the interfacial resistance between turns towards the adjacent turns. Furthermore, the turn-to-turn effective resistance is one order of magnitude greater than the longitudinal one. This favors the longitudinal flow of I_{op} through the winding. From the parameter R_c^{eff}, the effective turn-to-turn surface resistivity of the coil (ρ_{ct}^{eff}) can be assessed, as in [35]. This parameter follows the same trend as R_c^{eff}, going from 22 $\mu\Omega$ cm^2 at 4.7 K to 72 $\mu\Omega$ cm^2 at 80 K. This range is in agreement with the values found in different publications for defect-free NI coils [7], [33]–[36], [50]–[52], suggesting that the joints inserted in the winding have a limited impact on the characteristics of the prototype coil.

Finally, Fig. 4(c) shows the I_r^{eff}/I_{op} ratio, corresponding to the percentage of current flowing radially in the coil compared to the supplied I_{op}, for the same cases of Fig. 4(a) and (b). The value of I_θ^{eff}/I_{op} can be obtained as its complement. The effective radial current increases with the temperature (while the effective longitudinal current reduces correspondingly), in a range between 4.3% and 5.5% of the total operating current, despite the curves are not monotonic. In fact, comparing Fig. 4(a) and (b), R_θ^{eff} has a steeper increase with the temperature for the same $I_{op}^{\max}$, compared to R_c^{eff}. The value of R_θ^{eff} at 80 K is 3.8 times higher than that computed at 4.7 K, while R_c^{eff} increases by 2.1 times between the same values. This result agrees well with the expected behavior of NI windings, which favors the radial current flow when the longitudinal resistance rises (locally or globally), thus reducing the coil stability risks. Moreover, comparing the values found at the same temperature, I_r^{eff}/I_{op} rises with $I_{op}^{\max}$, although there are some exceptions, probably due to the measurements accuracy. This reflects the proportionality of the R_θ^{eff} parameter with the current, reported in Fig. 4(a). In fact, at low current amplitudes, the resistance of the superconducting layers in the damaged sections is minimal and the normal layers of the tape can contribute significantly to the current-sharing, despite their limited current carrying capacity. Increasing $I_{op}^{\max}$ at the same temperature, R_θ^{eff} rises while R_c^{eff} remains almost constant, which results in a greater portion of the transport current flowing in radial direction.

V. Conclusion

In this work, some defects are intentionally inserted into a pancake-wound NI HTS coil at specific locations in the form of lap joints, introducing high resistance sections which would impede the operation of insulated coils. The NI coil, instead, can be safely charged up to 70 A, at the maximum ramp-rate tested, equal to 5 A/s, in conduction cooling environment at temperatures between 4.7 K and 80 K. The magnetic field measured in its bore is constant with temperature and proportional to the current supplied, despite its amplitude results lower compared to the one expected in a defect-free coil. Overall, the tests proved how the defective NI coil can be properly operated at similar conditions than those achievable by its defect-free counterpart. An equivalent lumped parameter circuit is adopted to perform a straightforward analytical calculation of the relevant effective parameters of the winding at steady-state conditions. It can conveniently be applied to compare different working conditions of the same coil, as done in this work, or the performance of different NI coils. The model shows that, as the operating temperature increases, both the longitudinal and radial effective resistances of the coil increase, with the first rising more rapidly. A quote of the operating current, in the range between 4.3 and 5.5%, flows radially through the winding, thus guaranteeing its thermal stability. The realization of this prototype could demonstrate the feasibility of winding NI coils with tape segments cut from the same lot, potentially reducing the total conductor cost compared to the use of a single long piece of tape.

References

[1] S. Hahn, D. K. Park, J. Bascunan, and Y. Iwasa, "HTS pancake coils without turn-to-turn insulation," *IEEE Trans. Appl. Supercond.*, vol. 21, no. 3, pp. 1592–1595, Jun. 2011.

[2] S. Choi, H. C. Jo, Y. J. Hwang, S. Hahn, and T. K. Ko, "A study on the no insulation winding method of the HTS coil," *IEEE Trans. Appl. Supercond.*, vol. 22, no. 3, Jun. 2012, Art. no. 4904004.

[3] S. B. Kim *et al.*, "The normal-zone propagation properties of the non-insulated HTS coil in cryocooled operation," *Physica C: Supercond. its Appl.*, vol. 471, pp. 1428–1431, May 2011.

[4] A. Ikeda *et al.*, "Transient behaviors of no-insulation REBCO pancake coil during local normal-state transition," *IEEE Trans. Appl. Supercond.*, vol. 26, no. 4, Jun. 2016, Art. no. 4600204.

[5] A. Musso *et al.*, "Electrical characteristics of HTS coils with and with-out insulation in a layer-wound configuration," *IEEE Trans. Appl. Supercond.*, vol. 31, no. 5, Aug. 2020, Art. no. 4900605.

[6] H. Song and Y. Wang, "Simulations of nonuniform behaviors of multiple no-insulation (RE)$Ba_2Cu_3O_{7-x}$ HTS pancake coils during charging and discharging," *IEEE Trans. Appl. Supercond.*, vol. 26, no. 4, Jun. 2016, Art. no. 4700105.

[7] K. R. Bhattarai, K. Kim, S. Kim, S. Lee, and S. Hahn, "Quench analysis of a multiwidth no-insulation 7-T 78-mm REBCO magnet," *IEEE Trans. Appl. Supercond.*, vol. 27, no. 4, Jun. 2017, Art. no. 4603505.

[8] Z. Zhang *et al.*, "An experimental investigation of the transient response of HTS non insulation coil," *J. Supercond. Novel Magnetism*, vol. 30, pp. 387–393, Oct. 2016.

[9] T. Oki *et al.*, "Evaluation on quench protection for no-insulation REBCO pancake coil," *IEEE Trans. Appl. Supercond.*, vol. 26, no. 4, Jun. 2016, Art. no. 4702905.

[10] Y. Wang *et al.*, "An equivalent circuit grid model for no-insulation HTS pancake coils," *Supercond. Sci. Technol.*, vol. 28, Mar. 2015, Art. no. 045017.

[11] S. Noguchi, R. Miyao, K. Monma, H. Igarashi, H. Ueda, and A. Ishiyama, "Current behavior simulation in stacked NI REBCO pancake coils during local normal-state transition," *IEEE Trans. Appl. Supercond.*, vol. 27, no. 4, Jun. 2017, Art. no. 4603205.

[12] T. Wang *et al.*, "Analyses of transient behaviors of no-insulation REBCO pancake coils during sudden discharging and overcurrent," *IEEE Trans. Appl. Supercond.*, vol. 25, no. 3, Jun. 2015, Art. no. 4603409.

[13] G. Kim *et al.*, "A numerical method for spatially-distributed transient simulation to replicate nonlinear 'defect-irrelevant' behaviors of no-insulation HTS coil," *Supercond. Sci. Technol.*, vol. 34, no. 11, Sep. 2021, Art. no. 115004.

[14] Y. Kakimoto, T. Ichikawa, H. Onoshita, T. Kinpara, A. Ishiyama, and S. Noguchi, "Evaluation of electromagnetic behavior of no-insulation RE-BCO pancake coil with multiple defects," *IEEE Trans. Appl. Supercond.*, vol. 29, no. 5, Aug. 2019, Art. no. 4603005.

[15] S. Hahn *et al.*, "'Defect-irrelevant' behavior of a no-insulation pancake coil wound with REBCO tapes containing multiple defects," *Supercond. Sci. Technol.*, vol. 29, Sep. 2016, Art. no. 105017.

[16] U. Bong *et al.*, "'Defect-irrelevant-winding' no-insulation (RE)$Ba_2Cu_3O_{7-x}$ pancake coil in conduction-cooling operation," *Supercond. Sci. Technol.*, vol. 34, Mar. 2021, Art. no. 085003.

[17] K. Choi *et al.*, "Upper limit estimation of resistive heating made by no-insulation HTS magnet having defects," *IEEE Trans. Appl. Supercond.*, vol. 31, no. 5, Aug. 2021, Art. no. 4603005.

[18] Y. Yanagisawa *et al.*, "Basic mechanism of self-healing from thermal runaway for uninsulated REBCO pancake coils," *Phys. C*, vol. 499, pp. 40–44, Apr. 2014.
[19] Y. Wang *et al.*, "Self-protection mechanisms in no-insulation (RE)$Ba_2Cu_3o_x$ high temperature superconductor pancake coils," *Supercond. Sci. Technol.*, vol. 29, no. 4, Mar. 2016, Art. no. 045007.
[20] J. Song *et al.*, "Over-current quench test and self-protecting behavior of a 7 T/78 mm multi-width no-insulation REBCO magnet at 4.2 K," *Supercond. Sci. Technol.*, vol. 28, Sep. 2015, Art. no. 114001.
[21] W.D. Markiewicz *et al.*, "Quench analysis of pancake wound REBCO coils with low resistance between turns," *Supercond. Sci. Technol.*, vol. 29, Dec. 2015, Art. no. 025001.
[22] Y Suetomi *et al.*, "A novel winding method for a no-insulation layer-wound (RE)BCO coil to provide a short magnetic field delay and self-protect characteristics," *Supercond. Sci. Technol.*, vol. 32, Feb. 2019, Art. no. 045003.
[23] S. Hahn, D. K. Park, J. Voccio, J. Bascunan, and Y. Iwasa, "No-insulation (NI) HTS inserts for >1 GHz LTS/HTS NMR magnets," *IEEE Trans. Appl. Supercond.*, vol. 22, no. 3, Jun. 2012, Art. no. 4302405.
[24] D. Liu *et al.*, "Thermal stability and mechanical behavior in no-insulation high-temperature superconducting pancake coils," *Supercond. Sci. Technol.*, vol. 31, no. 8, Jul. 2018, Art. no. 085010.
[25] K. Katsumata *et al.*, "Influence of the turn-to-turn contact electrical resistance on the thermal stability in meter-class no-insulation REBCO pancake coils during a local normal-state transition," *IEEE Trans. Appl. Supercond.*, vol. 27, no. 4, Jun. 2017, Art. no. 4602005.
[26] K. Kim *et al.*, "Quench behavior of a no-insulation coil wound with stainless steel cladding REBCO tape at 4.2 K," *Supercond. Sci. Technol.*, vol. 30, May 2017, Art. no. 075001.
[27] N. C. Allen *et al.*, "Numerical and experimental investigation of the electromechanical behavior of rebco tapes," *IOP Conf. Ser.: Mater. Sci. Eng.*, vol. 102, 2015, Art. no. 012025.
[28] C. Senatore *et al.*, "Progresses and challenges in the development of high-field solenoidal magnets based on RE123 coated conductor," *Supercond. Sci. Technol.*, vol. 27, Sep. 2014, Art. no. 103001.
[29] V. Mosser *et al.*, "High-accuracy Hall-based sensors for high magnetic field applications," *Supercond. Sci. Technol., Proc. 21st Int. Magn. Meas. Workshop*, Grenoble, Jun. 24-28, 2019.
[30] [Online]. Available: www.ni.com/pdf/manuals/372425c.pdf
[31] Y. Yanagisawa *et al.*, "Basic mechanism of self-healing from thermal runaway for uninsulated REBCO pancake coils," *Physica C: Supercond.*, vol. 499, pp. 40–44, 2014.
[32] Y. Wang *et al.*, "An equivalent circuit grid model for no-insulation HTS pancake coils," *Supercond. Sci. Technol.*, vol. 28, no. 4, 2015, Art. no. 045017.
[33] M. Cho *et al.*, "Combined circuit model to simulate post-quench behaviors of no-insulation HTS coil," *IEEE Trans. Appl. Supercond.*, vol. 29, no. 5, Aug. 2019, Art. no. 4901605.
[34] S. An *et al.*, "Fast distributed simulation of 'Defect-Irrelevant' behaviors of no-insulation HTS coil," *IEEE Trans. Appl. Supercond.*, vol. 31, no. 5, Aug. 2021, Art. no. 4601605.
[35] X. Wang *et al.*, "Turn-to-turn contact characteristics for an equivalent circuit model of no-insulation ReBCO pancake coil," *Supercond. Sci. Technol.*, vol. 26, Jan. 2013, Art. no. 035012.
[36] S. Noguchi, R. Miyao, H. Okusa, T. Tatsuta, H. Ueda, and S. Kim, "Turn-to-Turn contact resistance measurement of no-insulation REBCO pancake coils," *IEEE Trans. Appl. Supercond.*, vol. 29, no. 5, Aug. 2019, Art. no. 4601605.
[37] Y Suetomi *et al.*, "Mechanism of notable difference in the field delay times of no-insulation layer-wound and pancake-wound REBCO coils," *Supercond. Sci. Technol.*, vol. 29, no. 10, Aug. 2016, Art. no. 105002.
[38] D. Liu *et al.*, "Numerical analysis of thermal stability and mechanical response in a no-insulation high-temperature superconducting layer-wound coil," *Supercond. Sci. Technol.*, vol. 32, Aug. 2016, Art. no. 044001.
[39] K. R. Bhattarai, K. Kim, S. Kim, S. Lee, and S. Hahn, "Quench analysis of a multiwidth no-insulation 7-T 78-mm REBCO magnet," *IEEE Trans. Appl. Supercond.*, vol. 27, no. 4, Jun. 2017, Art. no. 4603505.
[40] A. Ikeda *et al.*, "Transient behaviors of no-insulation REBCO pancake coil during local normal-state transition," *IEEE Trans. Appl. Supercond.*, vol. 26, no. 4, Jun. 2016, Art. no. 4600204.
[41] K. Yanagisawa *et al.*, "A long charging delay for a no-insulation REBCO layer-wound coil and its influence on operation with outer LTS coils," *IEEE Trans. Appl. Supercond.*, vol. 26, no. 4, Jun. 2016, Art. no. 4602304.
[42] X. Wang, T. Wang, E. Nakada, A. Ishiyama, R. Itoh, and S. Noguchi, "Charging behavior in no-insulation REBCO pancake coils," *IEEE Trans. Appl. Supercond.*, vol. 25, no. 3, Jun. 2015, Art. no. 4601805.
[43] S. Hahn *et al.*, "No-Insulation coil under time-varying condition: Magnetic coupling with external coil," *IEEE Trans. Appl. Supercond.*, vol. 23, no. 3, Jun. 2013, Art. no. 4601705.
[44] J. Geng *et al.*, "A parallel co-wound no-insulation (RE)BCO pancake coil for improving charging delays," *Supercond. Sci. Technol.*, vol. 32, no. 3, Jun. 2019, Art. no. 084002.
[45] S. Kim *et al.*, "Method for generating linear current-field characteristics and eliminating charging delay in no-insulation superconducting magnets," *Supercond. Sci. Technol.*, vol. 30, no. 3, Feb. 2017, Art. no. 035020.
[46] Y. G. Kim, S. Hahn, K. L. Kim, O. J. Kwon, and H. Lee, "Investigation of HTS racetrack coil without turn-to-turn insulation for superconducting rotating machines," *IEEE Trans. Appl. Supercond.*, vol. 22, no. 3, Jun. 2012, Art. no. 5200604.
[47] Y. G. Kim *et al.*, "Rotating permanent magnets based flux pump for HTS no-insulation coil," *IEEE Trans. Appl. Supercond.*, vol. 29, no. 5, Aug. 2019, Art. no. 5202106.
[48] M. N. Wilson, *Superconducting Magnets*. Oxford, U.K./New York, NY, USA: Clarendon Press/Oxford Univ. Press, 1983.
[49] J. W. Ekin, *Experimental Techniques For Low-Temperature Measurements – Cryostat Design, Material Properties, and Superconductor Critical-Current Testing*, Oxford, U.K.: Oxford Univ. Press, 2006.
[50] G. D. Yang *et al.*, "Characteristic resistance of no-insulation and partial-insulation coils with nonuniform current distribution," *IEEE Trans. Appl. Supercond.*, vol. 24, no. 3, Jun. 2014, Art. no. 7700405.
[51] Y. Liu *et al.*, "Study of contact resistivity of a no-insulation superconducting coil," *Supercond. Sci. Technol.*, vol. 34, Jan. 2021, Art. no. 035009.
[52] J. Lu *et al.*, "Contact resistance between two REBCO tapes: The effects of cyclic loading and surface coating," *Supercond. Sci. Technol.*, vol. 31, Jul. 2018, Art. no. 085006.